Optical Interference Effects in the Design of Substrates for Surface-Enhanced Raman Spectroscopy

LIAN C. T. SHOUTE, ADAM JOHAN BERGREN,* AMR M. MAHMOUD, KEN D. HARRIS, and RICHARD L. McCREERY*

Department of Chemistry, University of Alberta, Edmonton, Alberta, Canada (L.C.T.S., A.M.M., R.L.M.); and National Institute for Nanotechnology, National Research Council Canada, Edmonton, Alberta, Canada (L.C.T.S., A.J.B., K.D.H., R.L.M.)

This paper presents results showing that the design of substrates used for surface-enhanced Raman spectroscopy (SERS) can impact the apparent enhancement factors (EFs) obtained due to optical interference effects that are distinct from SERS, providing additional enhancement of the Raman intensity. Thus, a combination of SERS and a substrate designed to maximize interference-based enhancement is demonstrated to give additional Raman intensity above that observed for SERS alone. The system explored is 4-nitroazobenzene (NAB) and biphenyl (BP) chemisorbed on a nanostructured silver film obtained by vacuum deposition of Ag on thermally oxidized silicon wafers. The enhancing silver layer is partially transparent, enabling a standing wave to form as a result of the combination of the incident light and light reflected from the underlying Si substrate (i.e., light that passes through the Ag and the intervening dielectric layer of SiO_x). The Raman intensity is measured as a function of the thickness of the thermal oxide layer in the range from ~150 to ~400 nm, and despite a lack of morphological variation in the silver films, there is a strong dependence of the Raman intensity on the oxide thickness. The Raman signal for the optimal SiO_x interlayer thickness is 38 times higher than the intensity obtained when the Ag particles are deposited directly onto Si (with native oxide). To account for the trends observed in the Raman intensity versus thickness data, calculations of the relative mean square electric field (MSEF) at the surface of the SiO_x are carried out. These calculations are also used to further optimize the experimental setup.

Index Headings: **Raman spectroscopy; Surface-enhanced Raman spectroscopy; SERS; Silver island films; Interference.**

INTRODUCTION

A primary goal in the field of molecular electronics is utilization of the diverse electronic properties of molecules in order to realize improved and/or new functionality.[1–5] An important consequence of these quests is the need to demonstrate molecular behavior in a device, including the ability to separate contact effects from molecular processes.[4] A key to meeting this demand is a set of analytical tools that can provide information about molecular structure in a real device.[4] To this end, several techniques have been developed to investigate the spectroscopic properties of buried molecular layers.[6–10] Our group has demonstrated the use of Raman spectroscopy to correlate changes in the chemical structure of molecules in a junction to variations in electronic behavior.[11,12] However, this method is not generally applicable to most systems due to the low inherent sensitivity of Raman scattering and requires significant resonance enhancement to obtain sufficient sensitivity to monitor a thin (<5 nm) molecular layer sandwiched between a flat carbon surface and a partially transparent top contact. In order to build a more flexible toolbox of spectroscopic techniques for *in situ* characterization of buried interfaces without resonance Raman active molecules, we have been assessing the possibility of using surface-enhanced Raman spectroscopy (SERS).[13]

It is well known that extraordinarily strong enhancement of Raman scattering can be obtained when the molecule under study is located near the surface of a plasmonic moiety.[14–18] The characteristics of the surface plasmon (e.g., strength and excitation wavelength) are strongly correlated to the shape, size, and state of aggregation of the nanostructured surface. Many laboratories have investigated relationships between substrate characteristics, surface plasmon resonance (SPR), and SERS enhancement factors (EFs), as summarized in recent review articles.[16–20] These previous studies have demonstrated that to obtain an optimal EF, the wavelength of plasmon excitation should be tuned to both the electric field of the incident light and to that of the Stokes-shifted Raman scattered light. The design and fabrication of a variety of nanomaterials with large EFs have been recently reviewed.[19]

The main contribution to SERS originates from electromagnetic enhancement.[15] In this mechanism, incident light excites free electrons in the nanostructured metal into a collective oscillation (i.e., the electrons oscillate in resonance with the incident field), and the electric field around the nanostructure (upon which the molecule of interest resides) is amplified. A similar mechanism operates for the scattered radiation that can lead to further enhancement of the Raman intensity. Maximum SERS enhancement is achieved when the SPR maximum lies between the wavelengths of the excitation laser and the scattered radiation, since both are enhanced by the SPR. Because of these factors, tuning of the SPR by engineering metal nanostructures to maximize SERS EFs at a desired Raman excitation wavelength has become an important quest in developing analytical applications for SERS.[19,20] Most of the work in this area has been directed toward the optimization

Received 6 November 2008; accepted 4 December 2008.
* Authors to whom correspondence should be sent. E-mail: Adam.Bergren@nrc.ca, richard.mccreery@ualberta.ca.

0003-7028/09/6302-0133$2.00/0
© 2009 Society for Applied Spectroscopy

of SERS substrates by controlling the architecture of the nanostructures.[21] The most common variables employed to optimize and study SERS EFs are the size, spacing, shape, and dielectric environment of the nanoscopic features.[14,15,17,19–21] The support materials are typically designed to provide an appropriate template for the SERS substrate or to provide a different dielectric environment.[15]

In this paper, we prepare SERS substrates by electron beam evaporation of silver metal onto thermally oxidized Si. This procedure results in silver island films[22,23] that have modest SERS EFs ($\sim 10^5$ for adsorbed nitroazobenzene, or NAB), providing sufficiently large Raman signals such that high quality spectra can be obtained for non-resonance-enhanced chemisorbed molecules (e.g., biphenyl, or BP). Interestingly, however, the apparent EF also strongly depends on the thickness of an insulating oxide layer interposed between the Si substrate and the nanoscopic silver film. We interpret the relationship between the oxide thickness and the measured SERS EFs by considering the spatial distribution of the standing electric field produced from the propagation of light through the different phases of the support. The results indicate that by controlling the thickness of the oxide layer, the silver film morphology remains constant while the apparent SERS EF is modulated through optical interference effects. The results in this work are consistent with previous literature on interference enhanced Raman spectroscopy carried out using different systems, although these reports are few and scattered.[24–27]

EXPERIMENTAL

Disperse orange (90% technical grade, Sigma-Aldrich) was recrystallized twice from acetonitrile/water. The nitroazobenzene diazonium reagent was prepared as the tetrafluoroborate salt, as reported in detail elsewhere.[28,29] It has been shown by our group[13,30] and others[31] that diazonium reagents adsorb spontaneously to metals such as silver and copper. In this work, we employ silver substrates to enhance the Raman signal for nitroazobenzene (NAB) and we optimize the preparation conditions of the silver films deposited at thermally oxidized Si wafers in order to obtain reproducible and large EFs.[13]

Silicon wafers were thermally oxidized by flowing water-saturated nitrogen gas (thermostated at 96 °C) over silicon wafers in a 1000 °C furnace for 25 min. SiO_x of varying thickness are obtained along the direction of flow of the water/N_2 gas mixture. After oxidation, the wafers were diced into 1.4 cm × 1.8 cm chips. The silicon oxide layer thicknesses were determined by variable angle spectroscopic ellipsometry (J. A. Woollam Co., Inc.). This technique enables the thickness to be determined with better than 1 nm precision for films in the range of thicknesses studied (>100 nm) and therefore we have used three significant figures throughout the text. The Si/SiO_x chips were cleaned by successive sonication in acetone (HPLC, Fisher), 18 MΩ water (Millipore), and isopropanol (HPLC, Fisher) for 10 min each followed by drying in a directed stream of nitrogen.

Silver was deposited by electron beam evaporation at $\sim 10^{-6}$ Torr. The silver mass deposition rate and total thickness was varied by controlling the electron beam current (at 7.5 kV) and monitored with a quartz crystal microbalance. Atomic force microscopy (AFM, VEECO Digital Instruments 3100) was used in tapping mode to measure the surface roughness of the silver nanostructures. To prepare smooth silver films, a 100 nm layer of silver was deposited over a 4 nm chromium adhesion layer on the SiO_x surface. Silver films were modified with NAB by immersing the silver substrates in a 0.5 mM nitroazobenzene diazonium salt solution in acetonitrile for 1 s immediately after silver deposition, rinsing with neat acetonitrile, and drying in a stream of nitrogen. Based on a recent report,[32] this preparation procedure results in the impingement of ~4 monolayer equivalents of NAB onto the surface of the substrate. A measure of the uncertainty in impingement can be made by considering that for a 0.5 mM concentration, immersion times between 0.5 and 1.5 s give calculated impingement values of 3 to 5 monolayer equivalents.[32] Thus, this procedure should provide molecular layers of NAB with approximately constant surface concentrations from sample to sample.

Raman spectra were collected in back-scattering geometry with a custom Raman spectrometer,[33] equipped with a 50 mm f/1.8 Nikon camera collection lens, 2000 grooves/mm holographic reflection grating, and an Andor back-thinned charge-coupled device (CCD) detector cooled to −80 °C. Excitation utilized *p*-polarized light incident at 49° relative to the substrate normal (unless otherwise indicated) using an Argon ion laser at 514.5 nm (Coherent Innova 308). Raman scattered light was collected normal to the sample surface. The incident laser was focused with an 8.6 cm lens to a spot size of 17.2 μm diameter at the sample. The laser power at the sample was 180 μW (19 W cm^{-2}). The integration time is typically 0.2 s. A depolarizer (CVI Melles Griot) and holographic notch filter (Kaiser Optical System, Inc.) were positioned at the entrance slit of the spectrometer. EFs were determined as described below from the relative intensities of the Raman signal at 1140 cm^{-1} (phenyl-azo stretch) for NAB.

RESULTS AND DISCUSSION

Raman spectra and mode assignments for NAB in solution,[34] and of NAB covalently bonded to silver,[13] pyrolyzed photoresist film (PPF),[12,13,35] glassy carbon,[34] and other surfaces[30] have been reported previously. In order to extend our studies on the potential of SERS to follow structural changes in ensemble molecular electronics devices,[13] we began to design and optimize SERS substrates. This strategy utilizes determinations of the SERS EF, given by[15]

$$\text{SERS EF} = \frac{I_{surf}}{I_{soln}} \frac{N_{soln}}{N_{surf}} \quad (1)$$

where I_{surf} and I_{soln} are the experimentally measured Raman peak intensities (e mW^{-1} s^{-1}) for SERS and for the same molecular species in solution, respectively, and N_{soln} and N_{surf} are the number of molecules probed in solution and at the silver surface, respectively. In order to determine N_{soln}, the overlap between the laser excitation source and the collection volume of the spectrometer was estimated geometrically. Based on the 8.6 cm focal length lens and the 0.1 cm path length of the cell utilized, this collection volume is approximately 1.4×10^{-9} L. Thus, N_{soln} is 4.7×10^{12} molecules for a concentration of 5.7 mM NAB (this concentration was used in experiments as described below). N_{surf} is given by the number of NAB molecules in the spot size (17.2 μm radius) of the laser. N_{surf} can be estimated by considering the surface concentration of NAB (Γ_0, mol cm^{-2}) such that

$$N_{surf} = \Gamma_0 N_a A \quad (2)$$

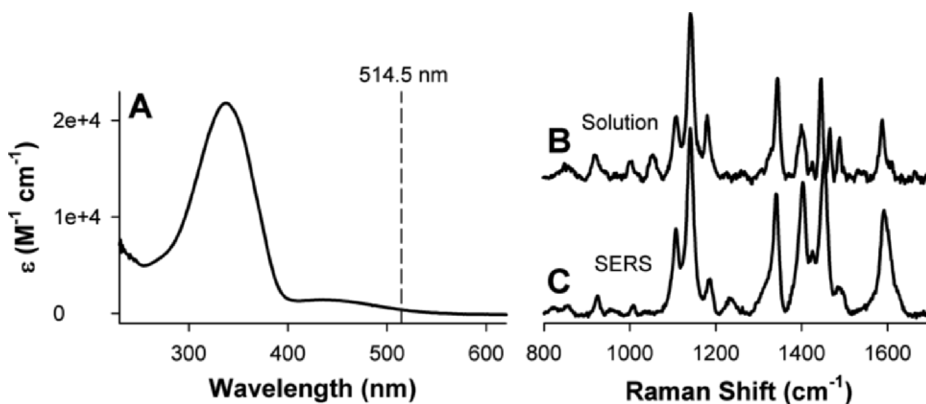

FIG. 1. (**A**) Extinction spectrum of NAB in solution, showing that pre-resonance enhancement is expected for 514 nm excitation. (**B**) Normal Raman spectrum of NAB in dimethyl sulfoxide. (**C**) SERS spectrum of NAB adsorbed at vacuum deposited silver supported on a thermally oxidized silicon wafer (Si/SiO_x).

where N_a is Avogadro's number and A is 9.3×10^{-6} cm^2 (the laser spot area). The coverage of a monolayer of NAB molecules is $\sim 1 \times 10^{-9}$ mol cm^{-2}.[36] Using this as an estimate of Γ_0, N_{surf} is 5.6×10^9 molecules of NAB (assuming one full monolayer). Although we have not attempted to measure the exact coverage of NAB, the impingement of NAB is kept fixed for all samples.

An extinction spectrum of NAB in solution is shown in Fig. 1A. The location of the 514 nm laser line utilized for excitation is indicated in the figure, showing that a significant pre-resonant enhancement is expected for NAB.[12,37] The Raman spectra of 5.7 mM NAB in DMSO solution and adsorbed at a nanostructured Ag island surface on Si/SiO_x are shown in Figs. 1B and 1C, respectively. The main features of these spectra are similar to those reported earlier.[12,13,34,35] By comparing spectra similar to those shown in Fig. 1 and employing Eq. 1, the SERS EF can be calculated in order to make various comparisons. However, for NAB, we have factored out contributions to the Raman signal due to molecular resonance. The potential utility of SERS for monitoring structural changes in "live" molecular electronic junctions containing a molecule that is not resonance enhanced is illustrated in Fig. 2. The extinction spectrum of biphenyl (BP) in solution is shown in Fig. 2A, with a vertical line indicating the excitation wavelength in Raman experiments. The position of the extinction band for BP relative to the 514 nm line shows that no resonant or pre-resonant enhancement is expected for BP. The solution-phase Raman spectrum for BP is shown in Fig. 2B. When BP is chemisorbed onto a flat Ag surface (100 nm Ag on 3 nm Cr), as shown in Fig. 2C, none of the bands for the molecule are detected above the noise. However, Fig. 2D shows that sufficient sensitivity is realized when using a silver island film on SiO_x to observe a Raman spectrum for BP.

Comparison of the SERS EF as a function of various experimental parameters was used as a guide in the design of the substrates in order to refine the system and obtain a reproducible and reliable response. To begin, we varied the total (nominal mass) film thickness (t) and deposition rate (r). Figure 3 shows a plot of the SERS EF as function of t (Fig. 3A) and r (Fig. 3B). As shown, the Raman intensity increases as t increases from 1 to 9 nm (Fig. 3A), and then falls off for thicker films. Thus, a total film thickness of 9 nm, as judged

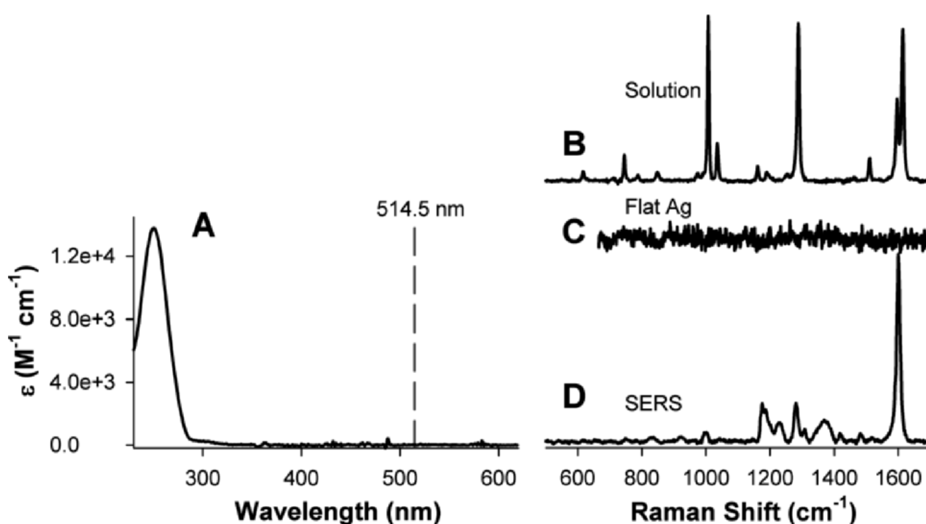

FIG. 2. (**A**) Extinction spectrum of BP in solution, showing that no resonance or pre-resonance enhancement is expected. (**B**) Normal Raman spectrum of 0.49 M BP in CH_2Cl_2 solution. (**C**) Raman spectrum of NAB adsorbed at a flat Ag sample (100 nm Ag on 3 nm Cr) showing only noise. (**D**) SERS spectrum of BP chemisorbed on an Ag island film on Si/SiO_x, showing that a thin molecular layer on a solid support can be detected through the increase in Raman intensity due to SERS.

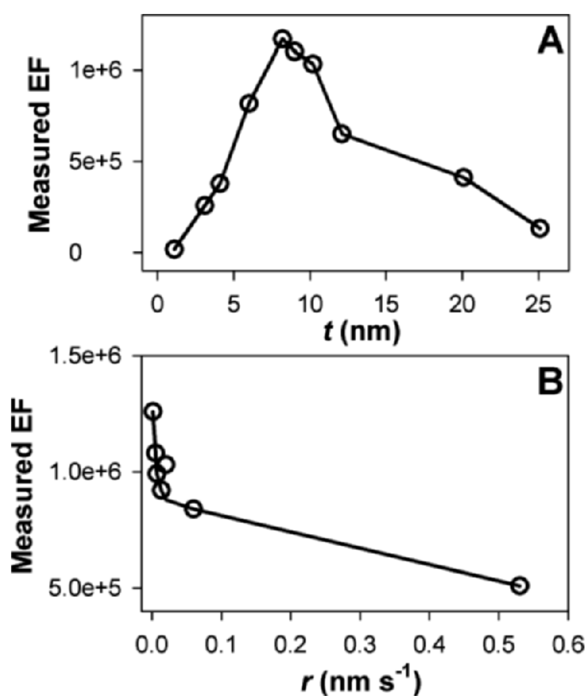

FIG. 3. (**A**) Effect of silver mass thickness (t) on SERS EFs calculated from the intensity of the 1140 cm^{-1} band (SiO_x thickness = 271 nm and $r = 0.02 \pm .01$ nm s^{-1}). (**B**) Effect of the deposition rate (r) on the SERS EFs (SiO_x thickness = 230 nm and $t = 9$ nm). The SERS EFs have standard deviations of ~15% for different samples (three independent samples) prepared with the same t and r values with <5% variation from spot-to-spot on the same sample (three spots). Lines are intended as a guide to the eye.

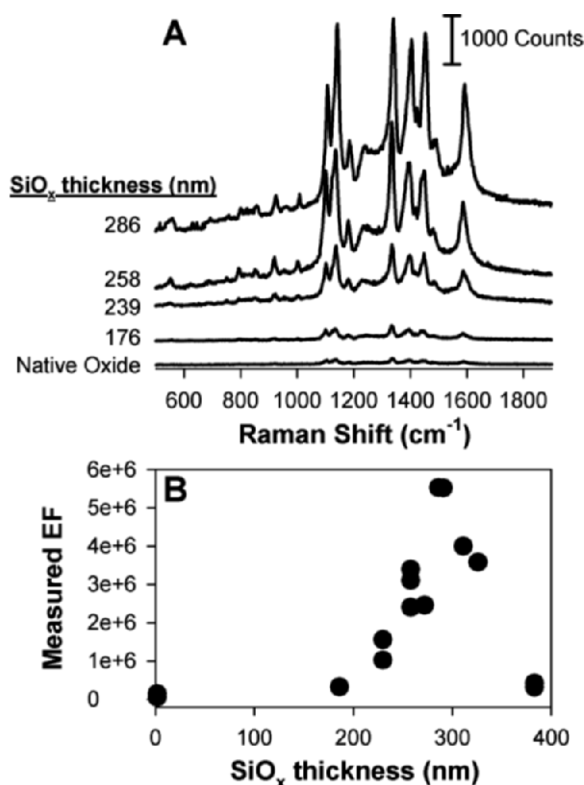

FIG. 4. Effect of silicon oxide (SiO_x) layer thickness on Raman intensity. (**A**) Raw Raman spectra for NAB chemisorbed at Ag island films deposited on a series of samples with different SiO_x thicknesses. (**B**) Corresponding calculated SERS EFs as a function of SiO_x thickness. Note that Raman spectra for SERS EF calculations were background subtracted. All silver films were prepared under identical conditions ($r = 0.02 \pm 0.01$ nm s^{-1} and $t = 9 \pm 0.1$ nm).

using a QCM monitor inside the evaporation chamber during deposition, was utilized as the optimal value (AFM characterizations of sample morphology reported in the supplementary information show a thickness of the Ag film between 5 and 12 nm results when the mass thickness is 9 nm). Figure 3B, on the other hand, shows that a progressively larger EF is obtained as r decreases. This effect was studied previously,[38] where it was shown that the morphology of the Ag film changes with deposition rate due to nucleation and growth dynamics. However, in order to balance signal enhancement and sample throughput, a value of 0.02 nm s^{-1} was chosen. This procedure is straightforward, reproducible (<5% relative standard deviation (RSD) for three spots on a single sample and 22% RSD for four independent samples), and yields substrates with moderately high values for the EF ($>10^5$).

Although the results shown in Fig. 2 demonstrate that the Ag island film substrates can be used to increase signal intensities into a range useful for characterizing molecules that are not resonance enhanced, during our initial optimizations of the substrate, the thickness of the underlying thermal oxide layer upon which the silver is deposited was found to modulate the value of the EF obtained, prompting a thorough evaluation of the effect. The variation in EF with SiO_x thickness was much larger than the sample-to-sample variability for a given thickness. A systematic study was initiated in which several samples were prepared with progressively thicker SiO_x layers, and Ag island films and NAB depositions were carried out in an identical fashion before determining the SERS EF obtained for each oxide layer thickness.

Figure 4 illustrates the effect of the thermal oxide layer thickness on the apparent EFs for NAB at a series of Ag island films where the underlying substrate is Si. In Fig. 4A, an overlay of the Raman spectra for several thicknesses of thermal oxide show that the Raman intensity changes dramatically with SiO_x thickness. Figure 4B draws out these differences by plotting the measured EF versus SiO_x thickness. For samples deposited directly on Si (with native oxide), the observed EF of $1.5(\pm 0.2) \times 10^4$ is at the lowest value observed for any of the SERS substrates. For samples that have a thermal oxide layer, the measured EF increases as a function of thickness until reaching a peak of $5.5(\pm 0.8) \times 10^6$ at an oxide thickness value of ~290 nm, and then decreases. For these experiments, the silver film was prepared under identical conditions and the modification of the surface with NAB was carried out in exactly the same manner (see the Experimental section). These experimental protocols reduce the possibility that the concentration of NAB on the surface of the silver film changes with oxide thickness. Moreover, the experimental error in the measured Raman intensities obtained for several samples prepared in an identical way is negligible compared to the changes in intensity that result when only the oxide layer thickness is altered. For example, for a series of four samples, each with a 258 nm SiO_x thickness, the measured EF is $2.7(\pm 0.6) \times 10^6$ (the reported error is the standard deviation, with $N = 4$). Thus, the variation from sample to sample spans a factor of 1.5 (at worst), while the changes in the measured EF as a function of SiO_x thickness span nearly a factor of 40 (from 1.47×10^5 to 5.53×10^6).

Several mechanisms underlying the dependence of EF on SiO_x thickness can be considered, including variations in the

TABLE I. Summary of results from threshold analysis of SEM images for silver island films deposited onto various substrates.

SiO_x thickness (nm)	Surface coverage (%)	Particle distribution (particles μm^{-2})	Characteristic diameter (nm)
0 (B-doped)	74.4	484	44
0 (no doping)	75.3	563	41
176	74	462	45
186	74.1	482	44
258	73.7	475	44
347	71.4	493	43
383	76.8	412	49
Average	74.2	482	44
Standard deviation	1.64	45	2.4
RSD (%)	2.2	9.3	5.5

morphology of the silver film for different SiO_x thicknesses, electronic coupling of the SPR of the silver film to the underlying Si substrate as modulated by the intervening SiO_x layer, and optical interference effects. Of these mechanisms, the first two involve variation of the SPR of the silver film, while optical interference patterns do not require any changes in the SPR in order to modulate the Raman intensity.

The morphology of silver films was assessed using scanning electron microscopy (SEM) and AFM for samples that varied only in SiO_x thickness. These results are presented in the supporting Supplemental Material (Figs. S-1 and S-2)[†] and are summarized in Table I. Table I lists the surface coverage, particle distribution, and diameter obtained from analysis of Fig. S-2 (see Supplemental Material) using image analysis software. The surface coverage is given by the average pixel gray scale values, while the particle distribution was obtained by manually counting the number of particles and dividing by the image area. Finally, the characteristic diameter of the particles was determined as an average by using the surface coverage factor and assuming a spherical shape for the particles. No trends in particle size or density were observed with variation of SiO_x thickness, with a mean particle size of 44 ± 2.4 nm for the entire thickness range considered. Importantly, no significant changes in Ag particle morphology were observed by either AFM or SEM with variation of SiO_x thickness, indicating that changes in morphology are not responsible for the modulation of the SERS EFs. These results leave electronic coupling and optical interference effects as the possible mechanisms, and electronic coupling is considered first.

Since the SERS substrates consisted of silver island films deposited onto a layer of SiO_x on a conducting Si layer (~ 0.1 Ω^{-1} cm^{-1}), electronic interactions between the silver film and the Si surface may be possible. Recent studies have shown that interparticle plasmon coupling can give rise to pronounced shifts in the SPR wavelength with respect to that observed for an isolated particle.[17,39,40] These investigations have shown that the coupling strength decays with the inverse cube of the separation distance between the plasmonic centers. Moreover, the SPR wavelength shift decay length is ~ 0.2 times the particle diameter. For our samples, the largest particle diameter is ~ 45 nm, giving a decay length of ~ 9 nm. This indicates that the oxide thicknesses used in this study (smallest = 174 nm) are too large for significant electronic coupling between the silver film SPR and the Si subsurface. This conclusion is reinforced by the observed increase of the ultraviolet–visible (UV-Vis) extinction maxima to longer wavelength as the SiO_x increases in thickness, contrary to the expectation for a coupling-induced effect (see Figs. S-3 to S-5 in the Supplemental Material). Finally, theories for the case of interactions between the surface plasmon resonances of a spherical particle and a planar metallic surface have been considered in detail.[16] For a system that considers a metal nanoparticle at some distance from a planar metal surface, the value of the electric field enhancement falls off rapidly as the separation distance between them increases. In fact, for separation distances approaching the radius of the particle, the value of the electric field intensity is only slightly higher than that for an isolated particle. A second coupling effect related to changes in the dielectric constant of the surrounding medium is also possible.[16,18] However, because the identity of the spacer layer (SiO_x) is constant, no significant change in the dielectric constant of the support with SiO_x thickness is expected.

After ruling out changes in the sample morphology and electronic coupling with oxide thickness, we return to an analysis of Fig. 4. Given the well-documented standing electric field profile that results when light is reflected from a conductive surface,[41–44] we have examined how this mechanism could lead to interference modulated Raman intensities. There are only a few reports that have considered interference effects in Raman spectroscopy.[24–27] Only one of these reports[25] combined SERS and interference enhancement by using a dielectric layer of SiO_x on a reflective material (Ag) to obtain enhancement from both. In that study, the dielectric layer thickness was varied between 0 and 150 nm, and an interference enhancement of ~ 6 was realized for 514.5/488 nm excitation or ~ 30 for 647.1 nm excitation. For our case, we analyzed the possibility that interference enhancement was responsible for the trends in Fig. 4 by carrying out calculations of the relative mean square electric field profiles at the air–SiO_x interface (at the location of the silver island film). These calculations utilized optical constants for the materials determined using variable angle spectroscopic ellipsometry or taken from the literature.[45] Using these values, optical absorbance and transmission spectra were simulated using FilmStar (www.ftgsoftware.com) software, and mean square electric field profiles were generated for a multilayered structure using theory for classical wave mechanics.

The results of the UV-Vis experiments (see Supplemental Material) indicate that the transmittance of a 9 nm silver film on quartz or glass is at least 30% at 514 nm, indicating that a significant portion of the incident light is transmitted to the underlying materials. As a consequence, a significant portion of the light incident on the Ag island surface will reach the underlying Si and be reflected from that surface back toward the SiO_x–Ag interface. The combination of incident and reflected light produces a spatially distributed standing electric field pattern. The characteristics of the standing wave are determined by the optical properties of the materials involved, the wavelength of the incident light, the incidence angle, and the thicknesses of the various phases.

Using FORTRAN programming, we have calculated mean square electric field (MSEF) profiles in a three-phase stratified medium consisting of Si, SiO_x, and air for 514.5 nm light. The algorithms are based on classical descriptions of light wave mechanics rooted in the plane traveling wave solutions to

† Supplemental Material is available on-line in the electronic version of the Journal (http://www.s-a-s.org).

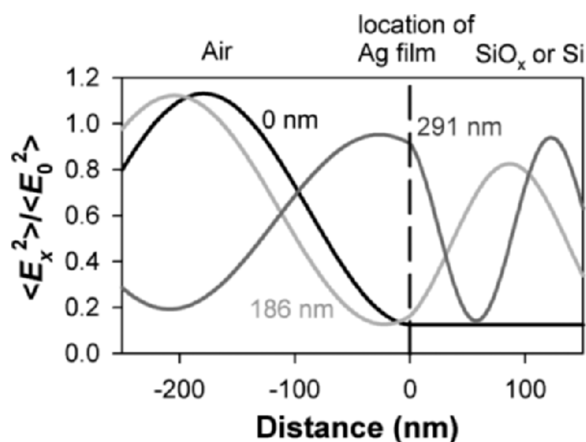

FIG. 5. Mean square electric field values in the *x*-direction for selected values of SiO_x thickness. Data calculated for a Si–SiO_x–air sample, where a distance value of 0 nm indicates the SiO_x–air interface that represents the location of the Ag film, negative distance values represent distance above the SiO_x–air interface, and positive distance values are distance into the substrate (Si or SiO_x). The thickness of the SiO_x layer is given next to each curve.

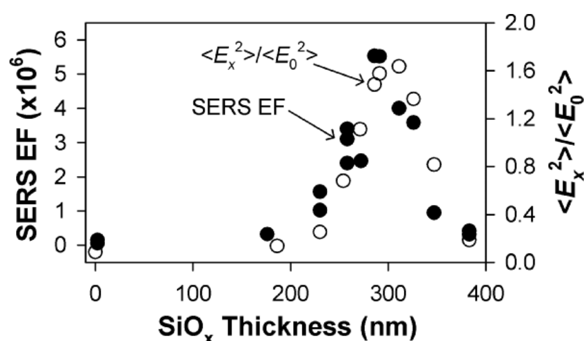

FIG. 6. Comparison of experimentally determined SERS EFs (solid circles) and the calculated relative mean square electric field values (open circles) at the SiO_x–Ag interface in the *x* direction as a function of SiO_x thickness. The stratified sample used in the calculation is Si–SiO_x–air.

Maxwell's equations and have been described in detail elsewhere.[46] The values of the MSEF calculated in this way represent the electric field intensity at any point within the stratified sample or above the SiO_x surface (no silver film was included in the calculation), with the thickness of the SiO_x layer varied in order to match the experimental values. Finally, the theoretically predicted MSEF values were calculated in three directions, denoted x, y, and z. The z component is along the surface normal, while the x and y axes both lie in the plane of the surface with the x direction coincident with the plane of incidence. Thus, *p*-polarized light has z and x components, while *s*-polarized light has only a y component.

Figure 5 shows an overlay of several $MSEF_x$ versus distance profiles for selected values of SiO_x thickness (0, 186, and 291 nm). In this plot, a distance value of 0 nm represents the air–SiO_x interface, which is the location of the silver film in SERS experiments, while negative distance extends into the region above the sample (air) and positive distance begins propagating through the SiO_x toward the underlying Si (or directly into the Si for 0 nm SiO_x thickness). The dashed line represents the interface at which the silver film is located. Thus, the value of the MSEF at this line is an important parameter due to the well-known dependence of the SERS intensity (I_{SERS}) on the magnitude of the electric field, as given by the proportionality

$$I_{SERS} \propto |E(\lambda_{ex})|^2 |E(\lambda_{sc})|^2 \quad (3)$$

where $E(\lambda_{ex})$ is the electric field at the excitation wavelength, and $E(\lambda_{sc})$ is the electric field at the wavelength of the scattered light. It is therefore apparent that the increase in the magnitude of the electric field resulting from the combination of the incident and reflected waves will have a large impact on the overall apparent SERS EFs that are measured. The results in Fig. 5 indicate that optical interference effects resulting from an interposing layer of insulating material can have a significant impact on the observed Raman intensity.

Figure 6 presents a summary of the calculated relative MSEF values (x direction, right ordinate, open circles) at the surface of SiO_x (where the nanostructured silver film is located) calculated for a series of SiO_x thickness values that matched those used in the experiments. Superimposed onto this plot are values for the SERS EFs (left ordinate, solid circles). Importantly, the trends observed for the relative MSEF values as a function of oxide layer thickness correlate strongly with the SERS EF data. Moreover, the correlation holds for the MSEF oriented in both directions along the long axis of the silver nanostructure (x and y directions, see Supplemental Material). These results indicate that the additional intensity of the electric field resulting from optical interference effects can significantly increase the apparent SERS EF.

Figure 7 summarizes the processes important in determining the Raman intensity on the stratified samples used in this work. First, the partially transparent Ag film allows light to be reflected from the underlying Si. The incoming waves then combine with the reflected waves to create a standing wave in the electric field that can act to increase or decrease the intensity of the Raman scattering. This interference-modulated effect is distinct from SERS arising from excitation of the SPR of the nanostructured Ag film from incident light only, which remains constant as the SiO_x thickness changes. However, the increase in the electric field due to interference can act to further excite the SPR of the silver films and subsequently lead to further increases in Raman intensity. Simply by changing the

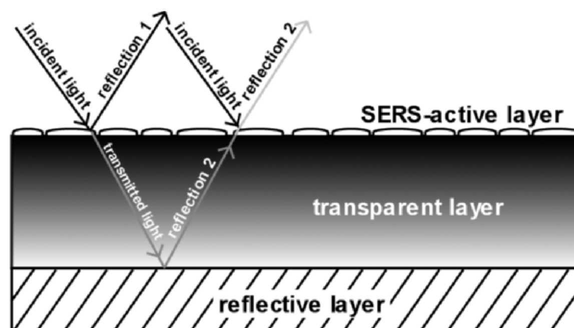

FIG. 7. Illustration of the interference effect that leads to increased Raman intensity over that obtained only for the SERS effect due to incident light. If the properties (e.g., thickness, refractive index) of the various phases are appropriate, extra intensity in the electric field is obtained through constructive interference between incident light and reflection from the underlying layer (reflection 2); this enhancement acts to further excite the SPR of the SERS-active silver island film, increasing the observed Raman intensity. The shading in the transparent layer represents the intensity of the standing wave electric field: as shown, it is highest at the location of the silver particles. Not to scale.

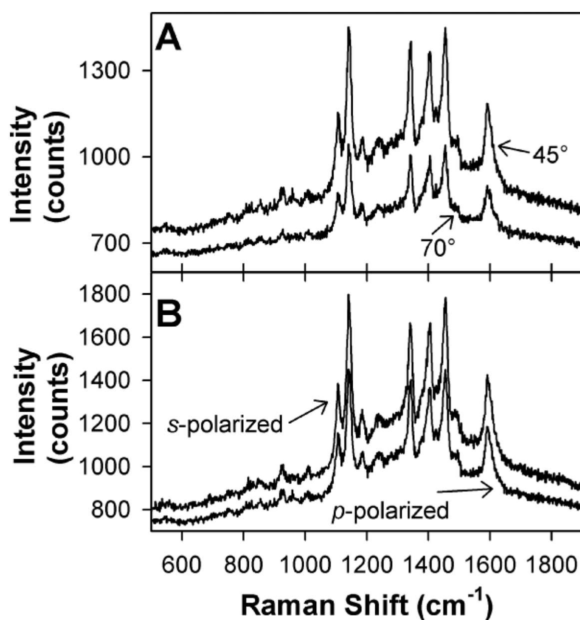

FIG. 8. SERS spectra for NAB adsorbed at an Ag island film on evaporated SiO_x (237 nm) on a reflective Ag substrate (100 nm). (**A**) Comparison of 45° and 70° angles of incidence, showing that 45° results in higher signal intensity, consistent with the predictions of theory. (**B**) Comparison of *s*- and *p*-polarized excitation (45° angle of incidence) showing that additional signal is obtained for *s*-polarized light, consistent with the predictions of the calculations. See text and Supplementary Material for more detail.

thickness of the inert, intervening SiO_x layer, the Raman intensity can be optimized for more enhancement than can be achieved through SERS alone. In Fig. 7, the case for constructive interference at the location of the silver film is shown. Thus, the shading in the transparent layer represents the intensity of the standing wave electric field, where it is highest at the location of the silver particles (with chemisorbed molecules).

A series of calculations were carried out in order to optimize the Raman intensity gains obtained through interference. As described in the Supplemental Material, the orientation of the electric field, the underlying reflector, and the angle of incidence were all considered. Based on the predictions of the calculations, experiments were carried out to serve as preliminary tests. For example, theoretical calculations predict that the interference pattern produces a much lower electric field at a near-glancing angle of incidence (70°) compared to the 45° angle used in the bulk of experiments; a corresponding reduction in the intensity of the Raman signal is expected. A second test of the theoretical predictions concerns the orientation of the electric field: *s*-polarized light (containing only the y component of the MSEF) yields a higher interference modulated electric field when using an Ag reflector than does *p*-polarized light (x and z components) and therefore should also yield a higher Raman signal intensity. More detail regarding these findings can be found in the Supplemental Material (Figs. S-6 to S-10); experimental validation of these predictions is presented below.

Figure 8 shows two overlays of SERS spectra for NAB adsorbed at a silver island film deposited onto a 237 nm evaporated SiO_x film on an Ag reflector (100 nm). Figure 8A shows that 45° yields a more intense Raman signal, as predicted by theory (see discussion above and the Supplemental Material). Figure 8B confirms that when using a silver layer as an underlying reflector, the signal intensity obtained for *s*-polarized excitation is slightly higher than that obtained using *p*-polarized excitation. Although it might be expected that due to the superior reflectivity of Ag relative to Si the overall signal might be larger when using Ag as a reflector, we have only observed a very small increase in signal. This may be due to changes in the morphology of the Ag islands, since they are deposited onto electron beam evaporated SiO_x films rather than on thermally oxidized wafers. AFM images of the e-beamed SiO_x layer show a much higher roughness factor (~3 nm rms roughness compared to ~0.5 nm for thermally oxidized SiO_x as measured using AFM). Due to the difference in sample morphologies, we cannot make any comparisons between the two types of samples. The results in Fig. 8B do, however, support the theoretical predication that the polarization of the incident light has a greater effect (detectable) with the more reflective substrate surface (Ag). Collectively, the results in Fig. 8 qualitatively demonstrate that interference modulation of the electric field intensity can be used to "tweak" the overall Raman signal intensity and that these changes can be qualitatively predicted by theory. We note that this analysis only takes into account interference-modulated electric field intensities; more complex changes in other parameters that may impact the observed SERS intensity are not considered.

CONCLUSION

This paper has demonstrated optical interference effects on the intensity of Raman signals obtained for molecules adsorbed at silver island films supported on thermally oxidized silicon wafers. As a result of light propagating through partially transparent, stratified phases, the electric field can be tuned simply by changing the thickness of an intervening layer that does not directly contribute to the SERS enhancement. The intensity of the electric field, independent of the enhancement obtained through surface plasmon effects, can be tuned by locating the SERS-active particles at a position of constructive interference between the incident and reflected light (see Fig. 7). The choice of materials must allow propagation of light through the SERS-active medium and through a transparent interlayer to an underlying reflector. In our case, the Raman signal for the optimal SiO_x interlayer thickness on Si is 38 times higher than the intensity obtained when the Ag particles are deposited directly onto a native oxide Si surface. The combination of SERS and interference enhancement, as shown in this paper, can therefore be utilized as an additional optimization strategy in order to provide higher signal intensities that may not be possible through changes in sample morphology or other methods that rely upon changes in the SPR. Further optimization of interference effects can either focus on utilizing different materials that have suitable optical properties or on changes in the experimental setup used to collect Raman spectra, as demonstrated briefly in this work.

ACKNOWLEDGMENTS

This work was supported by NSERC, the National Institute for Nanotechnology, and the University of Alberta. The National Institute for Nanotechnology is operated as a partnership between the National Research Council and the University of Alberta and is jointly funded by the Government of Canada, the Government of Alberta, and the University of Alberta. Portions of this work were carried out at the University of Alberta Nanofab facility. We thank Bryan Szeto for preparing samples of Si with different thicknesses of SiO_x and Marc D. Porter, Robert J. Lipert, and Jane McCreery for useful

discussions, including help with theoretical models and FORTRAN discussions, including help with theoretical models and FORTRAN programming.

SUPPLEMENTAL MATERIAL

The Supplemental Material mentioned in the text, including Figs. S-1 through S-10, is available on-line in the electronic version of the journal (http://www.s-a-s.org).

1. H. B. Akkerman and B. De Boer, J. Phys.: Condens. Matter **20,** 013001 (2008).
2. S. M. Lindsay and M. A. Ratner, Adv. Mater. **19,** 23 (2007).
3. R. McCreery, Chem. Mater. **16,** 4477 (2004).
4. R. L. McCreery, Anal. Chem. **78,** 3490 (2006).
5. R. M. Metzger, Chem. Rev. **103,** 3803 (2003).
6. M. W. Holman, R. Liu, and D. M. Adams, J. Am. Chem. Soc. **125,** 12649 (2003).
7. Y. Jun and X.-Y. Zou, J. Am. Chem. Soc. **126,** 13224 (2004).
8. L. G. Kaake, Y. Zou, M. J. Panzer, C. D. Frisbie, and X.-Y. Zhu, J. Am. Chem. Soc. **129,** 7824 (2007).
9. C. A. Richter, C. A. Hacker, and L. J. Richter, J. Phys. Chem. B **109,** 21836 (2005).
10. D. B. Robinson, J. R. Funamura, A. A. Talin, and R. J. Anderson, Appl. Phys. Lett. **90,** 083119 (2007).
11. R. McCreery, J. Wu, and R. P. Kalakodimi, Phys. Chem. Chem. Phys. **8,** 2572 (2006).
12. A. M. Nowak and R. L. McCreery, J. Am. Chem. Soc. **126,** 16621 (2004).
13. H. Liang, H. Tian, and R. L. McCreery, Appl. Spectrosc. **61,** 613 (2007).
14. C. L. Haynes, A. D. McFarland, and R. P. V. Duyne, Anal. Chem. **77,** 338A (2005).
15. K. A. Willets and R. P. Van Duyne, Annu. Rev. Phys. Chem. **58,** 267 (2007).
16. P. K. Aravind and H. Metiu, Surf. Sci. **124,** 506 (1983).
17. P. K. Jain, W. Huang, and M. A. El-Sayed, Nano Lett. **7,** 2080 (2007).
18. M. M. Wind, P. A. Bobbert, J. Vlieger, and D. Bedeaux, Physica A **143,** 164 (1987).
19. M. J. Banholzer, J. E. Millstone, L. Qin, and C. A. Mirkin, Chem. Soc. Rev. **37,** 885 (2008).
20. S. Lal, N. K. Grady, J. Kundu, C. S. Levin, J. B. Lassiter, and N. J. Halas, Chem. Soc. Rev. **37,** 898 (2008).
21. G. A. Baker and D. S. Moore, Anal. Bioanal. Chem. **382,** 1751 (2005).
22. W. B. Lacy, L. G. Olson, and J. M. Harris, Anal. Chem. **71,** 2564 (1999).
23. W. B. Lacy, J. M. Williams, L. A. Wenzler, T. P. Beebe, Jr., and J. M. Harris, Anal. Chem. **68,** 1003 (1996).
24. W. S. Bacsa and J. S. Lannin, Appl. Phys. Lett. **61,** 19 (1992).
25. H.-G. Bingler, H. Brunner, A. Leitner, F. R. Aussenegg, and A. Wokan, Mol. Phys. **85,** 587 (1995).
26. G. A. N. Connell, R. J. Nemanich, and C. C. Tsai, Appl. Phys. Lett. **36,** 31 (1980).
27. A. Lenac and M. S. Tomas, J. Raman Spectrosc. **22,** 831 (1991).
28. P. Allongue, M. Delamar, B. Desbat, O. Fagebaume, R. Hitmi, J. Pinson, and J.-M. Savéant, J. Am. Chem. Soc. **119,** 201 (1997).
29. D. L. Pavia, G. M. Lampman, G. S. Kriz, and R. G. Engel, *Organic Laboratory Techniques: A Microscale Approach* (Saunders College Publishing, New York, 1995), 2nd ed.
30. B. L. Hurley and R. L. McCreery, J. Electrochem. Soc. **151,** B252 (2004).
31. J. Pinson and F. Podvorica, Chem. Soc. Rev. **34,** 429 (2005).
32. G. A. Edwards, A. J. Bergren, E. J. Cox, and M. D. Porter, J. Electroanal. Chem. **622,** 193 (2008).
33. J. Ramsey, S. Ranganathan, R. L. McCreery, and J. Zhao, Appl. Spectrosc. **55,** 767 (2001).
34. T. Itoh and R. L. McCreery, J. Am. Chem. Soc. **124,** 10894 (2002).
35. A. M. Nowak and R. L. McCreery, Anal. Chem. **76,** 1089 (2004).
36. S. S. C. Yu, E. S. Q. Tan, R. T. Jane, and A. J. Downard, Langmuir **23,** 11074 (2007).
37. R. P. Kalakodimi, A. M. Nowak, and R. L. McCreery, Chem. Mater. **17,** 4939 (2005).
38. V. L. Schlegel and T. M. Cotton, Anal. Chem. **63,** 241 (1991).
39. L. Gunnarsson, T. Rindzevicius, J. Prikulis, B. Kasemo, M. Kall, S. Zou, and G. C. Schatz, J. Phys. Chem. B **109,** 1079 (2005).
40. K.-H. Su, Q.-H. Wei, X. Zhang, J. J. Mock, D. R. Smith, and S. Schultz, Nano Lett. **3,** 1087 (2003).
41. S. M. Stole and M. D. Porter, Appl. Spectrosc. **44,** 1418 (1990).
42. M. D. Porter, T. B. Bright, D. L. Allara, and T. Kuwana, Anal. Chem. **58,** 2461 (1986).
43. M. D. Porter, Anal. Chem. **60,** 1143A (1988).
44. D. D. Popenoe, S. M. Stole, and M. D. Porter, Appl. Spectrosc. **46,** 79 (1992).
45. D. W. Lynch and W. R. Hunter, "Optical Constants of Metals", in *Handbook of Optical Constants of Solids,* D. Palik, Ed. (Academic Press, San Diego, 1998).
46. A. N. Parikh and D. L. Allara, J. Chem. Phys. **96,** 927 (1992).